

# Descriptellation: Deep Learned Constellation Descriptors

Chunwei Xing<sup>\*1</sup>, Xinyu Sun<sup>\*1</sup>, Andrei Cramariuc<sup>1</sup>, Samuel Gull<sup>1</sup>, Jen Jen Chung<sup>2</sup>, Cesar Cadena<sup>1</sup>, Roland Siegwart<sup>1</sup>, Florian Tschopp<sup>3</sup>

**Abstract**—Current descriptors for global localization often struggle under vast viewpoint or appearance changes. One possible improvement is the addition of topological information on semantic objects. However, handcrafted topological descriptors are hard to tune and not robust to environmental noise, drastic perspective changes, object occlusion or misdetections. To solve this problem, we formulate a learning-based approach by modelling semantically meaningful object constellations as graphs and using Deep Graph Convolution Networks to map a constellation to a descriptor. We demonstrate the effectiveness of our Deep Learned Constellation Descriptor (*Descriptellation*) on two real-world datasets. Although *Descriptellation* is trained on randomly generated simulation datasets, it shows good generalization abilities on real-world datasets. *Descriptellation* also outperforms state-of-the-art and handcrafted constellation descriptors for global localization, and is robust to different types of noise. The code is publicly available at <https://github.com/ethz-asl/Descriptellation>.

## I. INTRODUCTION

A robot’s ability to estimate its precise pose in previously visited places is crucial for many applications, such as autonomous driving, trajectory tracking and robotic navigation. One crucial component for localization is a map which records landmarks and to which the robot can match its surroundings. Currently, many maps use appearance-based or object-based descriptors with metric information to represent visited places. Traditional appearance-based descriptors achieve good performance in local mapping, as demonstrated by e.g. ORB-SLAM2 [1] using DBOW [2]. They implement place recognition by selecting a candidate frame that most resembles the query frame, and estimate the pose through keypoints correspondences. However, localization systems based on visual keypoint descriptors, such as SIFT [3], SURF [4], BRIEF [5] and ORB [6], suffer from visual appearance changes due to changing viewpoints and occlusion, leading to candidate mismatches and further localization mistakes. Additionally, the storage requirement increases approximately linearly with the number of frames in the dataset, which limits system scalability on large-scale areas [7], [8].

Constructing maps with object-based descriptors is a proposed solution that uses high-level representations, such as lines [9], cubes [10], quadrics [11], and super quadrics [12]. The works [13], [14], which integrate SLAM with object

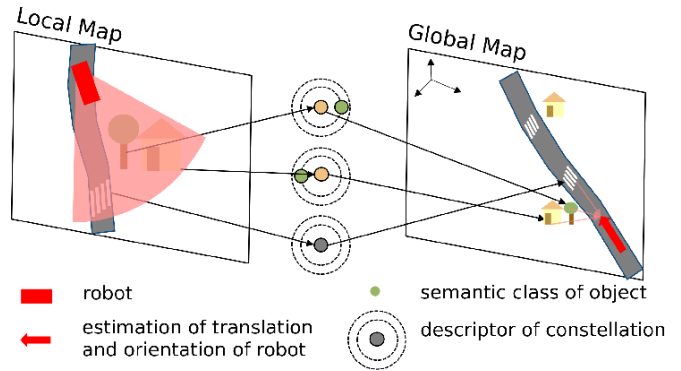


Fig. 1. Global localization based on semantic constellation descriptors. The global and local semantic object maps are described as object constellations. For each object in the global and local map, we generate a graph by specifying an edge between every pair of neighboring nodes according to the Euclidean distance. The graph is used to generate robust descriptors using GCNs.

detection, result in recognizable instance landmarks and inspire the construction of semantic object maps [14], ideal for robot localization in the presence of changing views and occlusion. Some proposed descriptors [9], [15], [16] use the semantic label directly as a descriptor. However, just the semantic label is often not distinct enough, especially when many objects of the same category are present. It is time-consuming to pair target and query objects with such aliasing descriptors. In contrast, a semantic constellation with structural cues, consisting of an object and its neighbors, is likely to be unique for a given scene [16], [17]. We map the structural and semantic information of an object constellation to a descriptor for global localization.

GCNs show great potential in solving complex constellation classification problems [18], [19]. In this work, we introduce a learning-based semantic constellation descriptor combining both geometric and semantic information. An overview of our method is shown in Figure 1. We extract object constellations from object-centric maps and construct graphs from them. We incorporate GCNs for representation learning from these graphs with embedded semantic information in each vertex to obtain descriptors for global localization. Our work can be divided into three main contributions:

- A graph-based learned descriptor of fused geometric and semantic information extracted from object constellations.
- A pipeline to train our deep-learned descriptor on simulation data and to deploy it to real-world applications.
- Comparisons on real-world datasets against existing baselines showing the feasibility and effectiveness of *Descriptellation* in terms of localization accuracy.

<sup>\*</sup> Authors contribute to the work equally.

<sup>1</sup> Authors are with the Autonomous Systems Lab, ETH Zurich, Switzerland. {chxing, xinsun, crandrei, sgull, cesarc, rsiegwart}@ethz.ch.

<sup>2</sup> Author is with School of ITEE, The University of Queensland, Australia [jenjen.chung@uq.edu.au](mailto:jenjen.chung@uq.edu.au).

<sup>3</sup> Author is with Arrival Ltd, United Kingdom, but the work was done while being a member of [f.tschopp@arrival.com](mailto:f.tschopp@arrival.com).

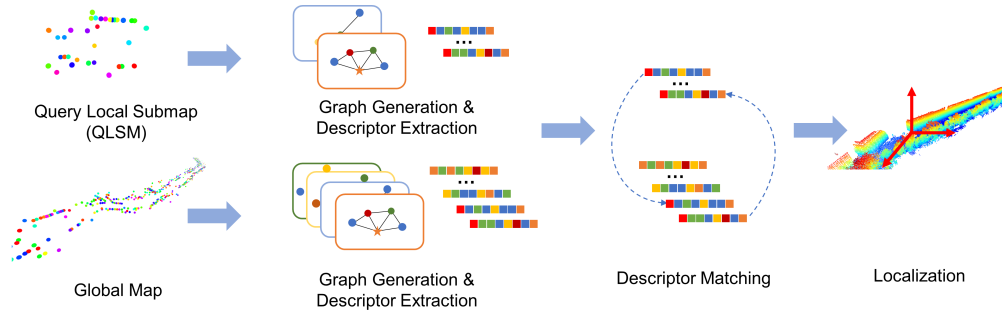


Fig. 2. Overview of the global localization system based on *Descriptellation*. For each object in the QLSM and the global map, a graph is built from the constellation of its neighboring objects, and its descriptor is extracted from the graph. By matching the descriptors in the QLSM with the database (descriptors extracted for each objects in the global map), candidate matching pairs can be found. By performing geometric verification on these matching pairs using RANSAC, a transformation matrix from the QLSM frame to the world frame can be obtained.

## II. RELATED WORK

### A. Descriptors for Global Localization

To achieve global localization, many descriptor generation methods exist, which typically trade off between distinctiveness and robustness. Distinctiveness reflects whether each landmark in a global map has an unique representation, which reduces the matching time when looking for pairwise correspondences. Robustness means that the same landmark’s descriptor should be consistent between maps and invariant to perspective changes, occlusion, and the passage of time. In terms of whether high-level structural information is included, descriptors can be categorized as *local* or *contextual*.

Local descriptors extract visual features around key-points [20], [21], or geometric features of segments [22]–[24] and show high reliability in place recognition. Contextual descriptors such as VLAD [25], PointNetVLAD [26], or 3D Gestalt [27] aggregate features from neighborhoods and are robust against noise. However, these descriptors are not rotation-invariant and perform poorly under viewpoint changes.

Recently, contextual descriptors from semantic graphs [17], [28] have been used for place recognition, achieving rotation-invariant performance in several datasets. Semantic objects form the nodes of the graph as 3D points, which can be connected by edges based on *e.g.* proximity. Such graphs contain both geometric and semantic information, and thus can be used to extract fused features that are more robust to the aforementioned changes [28]. Random Walk Descriptors (*RWalks*) [16], [17] achieve good performance on graph matching and localization. However, *RWalks* implicitly utilize the topological information of the graph instead of the explicit geometric information, and performance varies with the walk step count and graph complexity.

### B. Deep Learned Graph Descriptors

Inspired by the success of GCNs, graph embeddings learned by graph similarity networks are used to match two graphs built from semantic maps [28], [29]. The graph networks concatenate the spatial and semantic features extracted by two edge convolution networks directly as the graph embedding.

However, the geometric and semantic information could be combined as inputs and features extracted concurrently.

Graph representation learning methods can learn node-level and graph-level embeddings. Node-level embedding methods such as DeepWalk [30], node2vec [31], and Bag-of-Vectors [32] extract local graph structural information and project it onto lower dimensions. However, these methods lose the global structural information when extracting features. In this paper, we propose a graph-level embedding as the descriptor of an object by aggregating both node and edge features. GCNs extract structural information of neighboring nodes using spatial convolution operations.

In this paper, we use Deep Graph Convolution Networks (Deep GCNs) [33] to extract node features and use the global attention layer [34] to aggregate all the features extracted by Deep GCNs into a fixed-length graph-level embedding which can be used as a global descriptor.

## III. METHOD

In this section, we present our localization system based on *Descriptellation*. It leverages graph extraction from semantic object-centric maps (III-A) and graph matching using graph descriptors (III-B) for global localization (III-C). Figure 2 illustrates the overview of our system, focusing on the graph representation and matching.

Our goal is to localize a robot by matching the locally built map, called *Query Local Submap (QLSM)*, with a previously recorded *global map*. In both maps, each node (*i.e.* object) is assigned a learned descriptor by formulating its surrounding sub-constellation as a graph and extracting that graph’s features. Localization is achieved by matching descriptors of the QLSM to descriptors of the global map.

### A. Object Constellation Extraction and Graph Generation

The global and local semantic object maps are modeled as object constellations. For each object in the global and local map, we generate a graph by specifying an edge between every pair of neighboring objects (or nodes) according to the Euclidean distance within a predefined threshold, including the self-loop of the object itself. The threshold is defined by the average distance between two nodes in the global map.

## B. Network Architecture

As shown in Figure 3, our network is adapted from Deep GCN [33] consisting of the ResGCN backbone, a fusion block and a Multilayer Perceptron (MLP) prediction block. We modify the original network by adding an input embedding layer and an output global attention layer. The input of each node in the graph contains the 3D coordinates of its centroid  $(x, y, z)$  and an class label  $C$ . A standard one-hot encoding of the class label would considerably increase the size of the network. The ablation study on the input encoding methods refers to Section IV-G. We therefore preprocess the label by learning a 3-dimensional embedding  $e$ . To extract features from node embeddings and edges, we use a 14-layer ResGCN as a backbone, and a Max-Relative convolution layer. The fusion block consists of a fully connected layer with max-pooling.

In order to aggregate the embeddings of all the nodes into a graph-level fixed-length embedding, an attention layer [34] is used. It is a gated graph sequence neural network given by

$$\mathbf{r}_i = \sum_{n=1}^{N_i} \text{softmax}(h_{\text{gate}}(\mathbf{x}_n)) \odot h_{\theta}(\mathbf{x}_n), \quad (1)$$

where  $h_{\text{gate}}$  and  $h_{\theta}$  are neural networks,  $\mathbf{x}_n$  denotes the node features for node  $n$ ,  $N_i$  is the number of nodes for batch index  $i$ ,  $\mathbf{r}_i$  denotes the batch-wise graph-level output, and  $\odot$  denotes element-wise multiplication. We utilize the batch triplet loss [35] to optimize the parameters during training.

## C. Global Localization

To account for outliers and estimate a 3D transformation between the QLSM and the *global map* we use Random Sample Consensus (RANSAC) [36]. For each object descriptor in the QLSM, we find the corresponding  $K$  candidates with the closest descriptors in  $L2$  norm space in the *global map*. RANSAC then finds a 3D geometric registration between queries and candidates given the predefined minimum inlier threshold  $t_{\text{ransac}}$ . Addressing applications with observable gravity direction (e.g. ground vehicles or visual-inertial mapping) we assume a gravity-aligned local submap frame. Furthermore, the translation along  $z$  is negligible, and thus we only optimize for  $(x, y, \text{yaw})$ . Nevertheless, the full 6 Degrees of Freedom (DoF) poses are still recoverable using the same method if the application requires it.

## D. Simulated Training Dataset Generation

The training dataset is created in a simple simulation environment by stochastically generating a series of object-centric maps with different objects. A map is populated by superimposing randomly generated set of objects, using various geometric patterns: lines, circles, and multivariate normal distributions. The number of such patterns, the number of nodes in each pattern and the semantic labels of objects are sampled from a discrete uniform distribution. The relative coordinates of the patterns are sampled from a continuous uniform distribution.

Afterwards for each object, its constellation is first created as the anchor, by including the surrounding objects and with

the selected object as the center node. By transforming the anchor constellation using randomly sampled viewpoints, positive samples are obtained. A graph is then constructed from each constellation using the method illustrated in Section III-A. For the training and validation data, we generate 1000 anchor constellations and 9 positive constellations for each anchor using this strategy.

We simulate inconsistent observation of visited places, that happens in real-world scenarios, by adding noise when sampling the training data. This data augmentation additionally helps to prevent overfitting. We define  $\mathbf{p}_i$  as the 3D position of object  $i \in \mathbb{C}$  with respect to the origin of the constellation  $\mathbb{C}$ , and  $p_{i,\xi}$  is the position along the  $\xi$ -axis  $\in \{x, y, z\}$ .  $\mathcal{N}$  and  $\mathcal{U}$  denote normal distribution and uniform distribution respectively. We use the following augmentation methods:

- *Trans*: Translational noise is added to simulate the localization errors from upstream tasks, e.g. object mapping. This noise is added to each object in the constellation by

$$\tilde{\mathbf{p}}_{i,\xi} = p_{i,\xi} + \|\mathbf{p}_i\| \cdot e_{\text{trans}}, \quad (2)$$

- where  $\tilde{\mathbf{p}}_i$  defines a noisy position, and  $e_{\text{trans}} \sim \mathcal{N}(0, 0.25)$ .
- *Orient*: To simulate perspective changes, orientational noise is added to the whole constellation, i.e., the constellation is rotated around its origin by  $r \sim \mathcal{U}(-180^\circ, 180^\circ)$ .
- *Dropout*: This noise is used to simulate the *false negative* ratio of an upstream task, e.g. object detection. We remove an object with a probability  $e_{\text{dropout}} = 0.1$ .
- *FP*: This noise is implemented in the same context as *Dropout* noise, but instead represents the *false positive* ratio. We add a random object with a probability  $e_{\text{FP}} = 0.1$ .
- *Misclass*: Misclassification noise represents the upstream classification task error rate. We change the semantic label of each object  $i \in \mathbb{C}$  with a probability

$$e_{\text{misclass}} = \|\mathbf{p}_i\| / \max_{j \in \mathbb{C}} \|\mathbf{p}_j\| \cdot \alpha_{\text{misclass}}, \quad (3)$$

- where  $\alpha_{\text{misclass}} = 0.1$ .
- *Crop*: We crop the constellation by removing objects along the  $\xi$ -axis if

$$p_{i,\xi} > \max_{j \in \mathbb{C}} \|\mathbf{p}_j\| \cdot (1 - e_{\text{crop}}), \quad (4)$$

- where  $e_{\text{crop}} \sim \mathcal{U}(0, 0.3)$ .
- *Scale*: The scale noise is applied to the whole constellation. The coordinates of each object are scaled according to the same factor  $s \sim \mathcal{U}(0.85, 1.25)$ .

## E. Implementation

Our entire model is trained from scratch in an end-to-end fashion using the Adam optimizer [37] for 100 epochs, and the exponential decay rates  $\beta_1$  and  $\beta_2$  for the moment estimates are 0.9 and 0.999 respectively. The initial learning rate is  $1 \times 10^{-3}$ , and the decay rate is 0.7. The training took approximately 3 hours on a NVIDIA GeForce GTX 1060 Ti GPU and 6 Intel i7-8750H CPU.

We use the *topK* ratio as a target objective to stop the training and select the best model. More specifically, at the end of each epoch for all constellation embeddings in

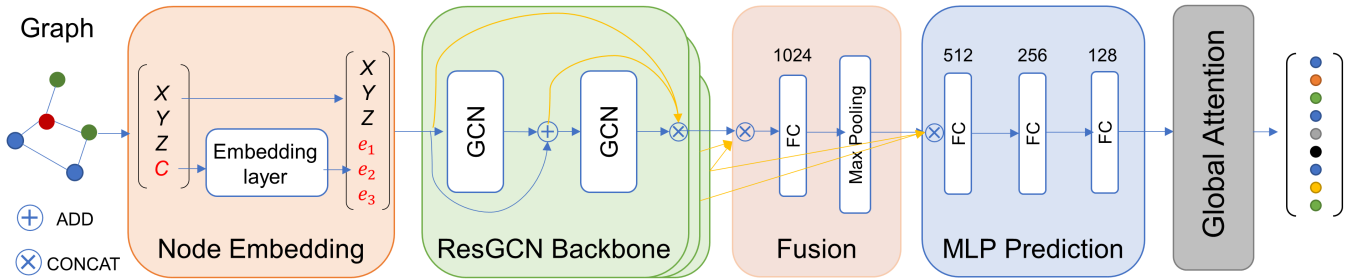


Fig. 3. Network architecture: Given a graph constructed according to Section III-A, the network integrates the spatial and semantic information of the edges and nodes to generate a graph descriptor using an extension of the Deep GCN architecture [33]. The numbers above the fully connected (FC) blocks represent output sizes.

the dataset, the  $K$  closest embeddings among all the other constellations are selected. The *topK* ratio is defined as the ratio of samples where at least one of the  $K$  selected embeddings has a matching label. The *topK* ratio strongly relates to the localization efficiency since the effectiveness of RANSAC highly depends on the number of false candidates it has to sort through.

#### IV. EXPERIMENTS

##### A. Datasets

To test the localization performance of *Descriptellation* on real world scenarios, we use two outdoor point cloud datasets: Paris-Rue-Lille [38] and IQmulus [39]. These datasets contain fine-grained point cloud data captured in a driving scenario, with semantic and instance annotations.

TABLE I  
DATASET STATISTICS, BEFORE AND AFTER PREPROCESSING.

Trajectory	Length	Original		Preprocessed	
		Objects	Classes	Objects	Classes
Lille1	1150 m	1349	39	795	25
Lille2	340 m	501	29	274	19
Paris	450 m	629	41	306	23
IQmulus	200 m	414	22	152	13

The Paris-Rue-Lille [38] is an urban dataset, containing 3 trajectories: Lille1, Lille2, and Paris. The IQmulus database [39] is scanned from a dense urban environment. The dataset statistics are summarized in Table I.

Dynamic objects, such as pedestrians and cars, are removed in pre-processing since we do not consider them relevant for localization. We want to focus on objects we will be able to redetect when revisiting the place. Similarly, unknown object categories are also removed. In addition to removing semantically dynamic objects, we also remove the “bollard” objects from the dataset, because we find the distribution of these objects is very dense across the whole dataset and they appear in very repetitive patterns. While *Descriptellation* still outperforms the other methods when using “bollards”, their addition decreases the performances of all baselines significantly due to heavy self-similarity. We represent the remaining objects using a 3D point located in the object’s centroid.

##### B. Experiment Setup

1) *Object-centric Maps Generation*: We generate object-centric maps from the point cloud datasets. The densely segmented global point cloud map is downsampled into voxels, each including 3D coordinates, an instance ID, and a semantic class label. The centroid of an object is computed as the mean coordinates of voxels with the same instance ID. The global map is then composed of all these object centroids. Each *semantic object* is then represented by the 3D centroid coordinates, the instance ID and the semantic class label. To extract descriptors for an object, we retrieve a local constellation for each *semantic object* in the global map. The local constellation is defined as a union of the object itself and its neighboring objects within a visual range threshold.

2) *Data Collection*: When collecting the test data, we randomly sample query positions and orientations on the predefined sampling trajectory in the object-centric map. For each query position, we take the current visible static objects from the query position within a visual range threshold to construct the *QLSM*, and we remove occluded objects [40]. We set the default visual range threshold to 30 m. The coordinates of each object in the map are transformed into local coordinates with a random yaw angle to simulate the observation at an unknown orientation. Object constellation extraction and graph generation then follow Section III-A.

3) *Testing Scenarios*: We propose 3 experiment cases to test the global localization performance of *Descriptellation*.

- *Self-localization*: In this experiment we use unpoluted data in the *QLSM*. This scenario represents testing with a perfect upstream object mapping system.
- *Fewer Objects*: To simulate the realistic scenario where objects are deficient or they could only be reached in a limited range, we reduce the visual range threshold to 20 m from the centric object when building the *QLSM*.
- *Added Noise*: Since the trajectories of the dataset were collected only once, to represent a more realistic localization scenario, we introduce different kinds of noise, including *Trans*, *Dropout*, *Misclass*, and *Scale*. The noise is implemented in the same way as described in Section III-D. For the *Trans* and *Scale* noises, we choose the error rate  $e_{trans} \sim \mathcal{U}(0, 0.1)$  and scale ratio  $s \sim \mathcal{U}(0.9, 1.1)$ . For the *Dropout* and *Misclass* noises, considering the accuracy of state-of-the-art object detection and image classification models [41], we choose  $e_{dropout} = 0.1$  and  $\alpha_{misclass} = 0.2$ .

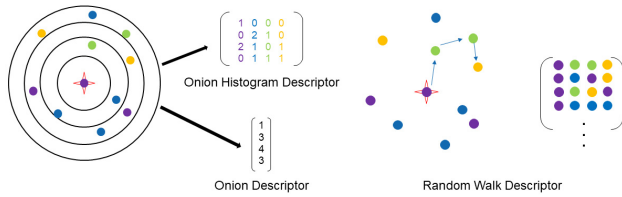


Fig. 4. Handcrafted baseline descriptors. The onion and onion histogram descriptor example shows the case when the number of shells  $n_s = 4$  and number of classes  $n_c = 4$ . The random walk descriptor example shows the case when the walk length  $l_w = 4$ .

### C. Baselines

We compare *Descriptellation* to five handcrafted descriptors: Onion Descriptor (*Onion*), Onion Histogram Descriptor (*OHist*) [42], Random Walk Descriptor (*RWalk*) [17], Graph of Semantics Matching - Graph Descriptor (*GOSG*) [43], and Graph of Semantics Matching - Vertex Descriptor (*GOSV*) [43]. Additionally, we also compare to two learned descriptors: PointNet Descriptor (*PNet*) [44], and Semantic Graph Networks Descriptor (*SGNet*) [28].

Illustrations of how the handcrafted descriptors work are shown in Figure 4. For Onion Descriptor (*Onion*) and Onion Histogram Descriptor (*OHist*), objects are split into  $n_s$  shells with equal spacing,  $d_s$ , between two neighboring shells. *Onion* counts the number of objects in each shell as the descriptor, and *OHist* creates a histogram of objects’ semantic classes instead. Graph of Semantics Matching - Vertex Descriptor (*GOSV*) shares a common format with *OHist*, but instead of counting semantic objects within a certain distance, it counts all the vertices in the whole QLSM [43]. Similarly, Graph of Semantics Matching - Graph Descriptor (*GOSG*) counts all the edges and bins them by edge type and distance [43]. For *RWalk*, a number of  $n_w$  random walks of length  $l_w$  are sampled starting from the query object. The semantic class labels of the visited objects are then stored in a descriptor matrix of shape  $n_w \times l_w$ .

We tune the parameters of the handcrafted baseline descriptors on simulation data. For *Onion* and *OHist*, we chose  $n_s = 3$  and  $d_s = 10\text{m}$ . For *RWalk*, we chose the walk length  $l_w = 4$  and the number of walks  $n_w = 30$ . We keep the parameters the same as in the original paper for *GOSG* and *GOSV* [43]. For PointNet Descriptor (*PNet*), we adapt the original PointNet++ [44] by removing the soft-max layer at the end of the network and train it using the same data, loss, and metrics as *Descriptellation*. For *SGNet*, we use the best pre-trained model for evaluation by remapping the semantics.

### D. Evaluation Metric

We evaluate the global localization performance by the success rate defined on the translation errors. In detail, the success rate  $\eta$  is defined as the ratio of localized samples whose translation errors are less than 1 m.

### E. Global Localization Performance

We sampled 500 query positions from each dataset and follow the pipeline described in Section III to compute the

TABLE II

GLOBAL LOCALIZATION PERFORMANCE ON THE LISTED DATASETS. THE BEST DESCRIPTOR IN EACH SCENARIO IS HIGHLIGHTED IN BOLD TEXT.

Traj	Metrics Scenarios	Translation Success Rate( $\eta$ ) [%]		
		Self-localization	Fewer Objects	Added Noise
Lille1	<i>Onion</i>	4.00 $\pm$ 0.31	1.48 $\pm$ 0.57	0.00 $\pm$ 0.00
	<i>OHist</i> [42]	96.80 $\pm$ 0.80	90.88 $\pm$ 1.13	32.36 $\pm$ 0.91
	<i>RWalk</i> [17]	93.24 $\pm$ 1.94	82.64 $\pm$ 0.81	40.92 $\pm$ 1.51
	<i>GOSG</i> [43]	70.08 $\pm$ 0.93	58.08 $\pm$ 0.57	7.80 $\pm$ 1.12
	<i>GOSV</i> [43]	91.72 $\pm$ 0.60	79.48 $\pm$ 0.16	30.44 $\pm$ 1.49
	<i>PNet</i> [44]	6.92 $\pm$ 0.48	4.32 $\pm$ 0.68	1.08 $\pm$ 0.30
	<b>Ours</b>	<b>99.60 <math>\pm</math> 0.22</b>	<b>92.08 <math>\pm</math> 0.63</b>	<b>41.00 <math>\pm</math> 1.06</b>
Lille2	<i>Onion</i>	15.32 $\pm$ 0.60	11.48 $\pm$ 1.31	1.04 $\pm$ 0.32
	<i>OHist</i> [42]	99.68 $\pm$ 0.24	98.84 $\pm$ 0.27	40.56 $\pm$ 0.97
	<i>RWalk</i> [17]	97.88 $\pm$ 0.95	95.64 $\pm$ 1.08	49.32 $\pm$ 1.53
	<i>GOSG</i> [43]	63.16 $\pm$ 0.73	57.36 $\pm$ 0.88	7.44 $\pm$ 0.29
	<i>GOSV</i> [43]	94.48 $\pm$ 0.37	90.20 $\pm$ 0.66	28.84 $\pm$ 0.67
	<i>PNet</i> [44]	22.40 $\pm$ 1.39	20.64 $\pm$ 0.77	2.96 $\pm$ 0.34
	<b>Ours</b>	<b>99.80 <math>\pm</math> 0.13</b>	<b>98.88 <math>\pm</math> 0.20</b>	<b>51.96 <math>\pm</math> 0.71</b>
Paris	<i>Onion</i>	10.20 $\pm$ 0.52	4.20 $\pm$ 0.51	2.20 $\pm$ 0.38
	<i>OHist</i> [42]	<b>96.60 <math>\pm</math> 0.55</b>	<b>80.12 <math>\pm</math> 0.91</b>	<b>47.24 <math>\pm</math> 1.55</b>
	<i>RWalk</i> [17]	91.32 $\pm$ 1.48	70.16 $\pm$ 2.60	46.96 $\pm$ 3.01
	<i>GOSG</i> [43]	74.08 $\pm$ 0.57	34.80 $\pm$ 0.68	10.48 $\pm$ 0.48
	<i>GOSV</i> [43]	87.04 $\pm$ 0.74	54.68 $\pm$ 0.56	31.72 $\pm$ 1.61
	<i>PNet</i> [44]	12.00 $\pm$ 1.04	5.28 $\pm$ 0.45	3.04 $\pm$ 0.64
	<b>Ours</b>	93.24 $\pm$ 0.64	67.00 $\pm$ 0.92	41.12 $\pm$ 0.47
IQmulus	<i>Onion</i>	75.92 $\pm$ 0.68	30.20 $\pm$ 1.24	42.68 $\pm$ 1.79
	<i>OHist</i> [42]	<b>99.40 <math>\pm</math> 0.22</b>	69.68 $\pm$ 1.31	66.04 $\pm$ 1.38
	<i>RWalk</i> [17]	95.68 $\pm$ 2.24	67.32 $\pm$ 2.37	64.00 $\pm$ 3.34
	<i>GOSG</i> [43]	8.08 $\pm$ 0.35	16.76 $\pm$ 0.74	1.12 $\pm$ 0.10
	<i>GOSV</i> [43]	31.36 $\pm$ 0.54	31.08 $\pm$ 0.24	13.32 $\pm$ 1.34
	<i>PNet</i> [44]	43.60 $\pm$ 1.44	19.20 $\pm$ 0.88	30.00 $\pm$ 1.08
	<b>Ours</b>	98.08 $\pm$ 0.24	<b>70.20 <math>\pm</math> 1.12</b>	<b>66.40 <math>\pm</math> 0.67</b>

estimated poses. Table II shows the localization performance of *Descriptellation* compared to the baselines on the Paris-Rue-Lille and IQmulus datasets. On Lille1 and Lille2, *Descriptellation* performs much better than the other descriptors in all cases. On Paris, *Descriptellation* shows a general performance among the top3 descriptors. On IQmulus, while not strictly outperforming all baselines, *Descriptellation* still shows the best overall performance and shows competitive results in all testing scenarios. In contrast, *GOSG*, *Onion* and *PNet* perform poorly in all cases.

On Lille1, in the *Self-localization* scenario, *RWalk*, *OHist* and *GOSV* have the descriptiveness to identify the constellations. However, since these descriptors only take vague spatial relations into account instead of specific dis-

TABLE III

COMPUTATIONAL TIME RESULTS. COMPUTE, MATCH, AND TOTAL REFER TO AVERAGE DESCRIPTOR COMPUTING, MATCHING AND TOTAL TIME IN S.

	<i>Onion</i>	<i>OHist</i>	<i>RWalk</i>	<i>GOSG</i>	<i>GOSV</i>	<i>PNet</i>	<i>SGNet</i>	<b>Ours</b>
Compute	0.014	0.015	<b>0.005</b>	0.138	0.022	0.006	0.063	0.243
Match	9.523	3.415	3.986	10.307	4.33	8.594	6.08	<b>2.63</b>
Total	9.537	3.430	3.991	10.445	4.352	8.600	6.143	<b>2.873</b>

tances among objects in the constellation, their descriptiveness can be weak when the number of spatial relations decreases. This causes the significant decrease in localization accuracy in the *Fewer Objects* scenario. In contrast, *Descriptellation* learns directly from the graph with specific distances between each pair of objects. The descriptiveness is still powerful even if the constellations contain fewer semantic objects because the distances between objects are actively used in the feature extraction. In the *Added Noise* scenario, all descriptors’ performances decrease. However, *Descriptellation* still performs the best thanks to being exposed to all kinds of noise during training.

Compared to *Lille1* and *Lille2*, *IQmulus* and *Paris* have much fewer objects and a shorter length, reducing the statistical strength of these experiments. Besides, for the *IQmulus* dataset, the object density reduces after removing the densely distributed “bollard” objects. The performance of *RWalk*, *OHist* and *Descriptellation* is much lower than on the *Lille1* datasets in the *Fewer objects* experiment, with greater similarity across the methods. This shows the influence of the object density and the distribution on the performance. The ambiguity may result from the self-similarity of the constellations or visual aliasing at different places. When the object distributions are similar to each other at different places, none of the tested methods are able to tell them apart and *Descriptellation* cannot extract more distinct descriptors from these constellations. Nevertheless, *Descriptellation* still shows robustness against noise and performs generally well among the top3 descriptors.

#### F. Computational Efficiency

Our experiment includes two evaluation phases, i.e., computing descriptors, and matching them with geometric verification. We compare the average timing on all the datasets for all the testing scenarios on an Intel(R) Core(TM) i7-8750H CPU. The results are summarized in Table III.

*PNet*, *SGNet*, *Descriptellation* and *GOSG* take longer computing time since they are computed iteratively for each object. In contrast, *Onion*, *OHist* and *RWalk* are computed once altogether for all objects. *PNet* and *SGNet* are faster thanks to batch computing. *Descriptellation* is still comparable with *GOSG* where batch computing is missing as well.

*Descriptellation* costs the shortest matching time thanks to its great distinctiveness.

#### G. Ablation Study

We explore how to combine geometric information and semantic information by setting up experiments on different

TABLE IV

TRAINING RESULTS WITH DIFFERENT MODEL INPUTS.

Model Inputs	Metrics			
	train loss	val loss	train top5	val top5
$(x, y, z)$	0.145	0.148	67.2%	81.7%
$(x, y, z, C_{integer})$	0.123	0.126	85.7%	94.4%
$(x, y, z, C_{onehot})$	<b>0.0786</b>	0.145	98.9%	90.0%
$(x, y, z, C_{embed})$	0.0805	<b>0.102</b>	<b>99.1%</b>	<b>98.1%</b>

input types for our model with the same backbones and attention layers. The input types are as follows:

- $(x, y, z)$ : only contains geometric information, i.e. the coordinates of the object. This serves as a baseline for the value of semantic information.
- $(x, y, z, C_{integer})$ : besides geometric information, also contains semantic information encoded by a scalar integer  $C_{integer} \in \{1, 2, \dots, N_{class}\}$ .
- $(x, y, z, C_{onehot})$ : encodes semantic information with a one-hot encoding, i.e.  $C_{onehot} \in \{0, 1\}^{N_{class} \times 1}$ .
- $(x, y, z, C_{embed})$ : encodes semantic information with a learnable embedding  $C_{embed} \in \mathbb{R}^{N_{embed} \times 1}$ . We use  $N_{embed} = 3$  in our experiments.

We can conclude from Table IV that the combination of geometric and semantic information is better than only using geometric information. Furthermore, a reasonable way to combine the geometric and semantic information is to first learn an embedding for the semantic class, and then concatenate it together with the geometric coordinates. We use this embedding-format model trained on the simulated training dataset to infer descriptors for global localization. As we choose an embedding that is much smaller than the one-hot encoding of the classes we save significant resources in the ResGCN backbone.

## V. CONCLUSION

In this paper, we presented a GCN architecture based on Deep GCNs and the attention mechanism to learn a set of object constellation descriptors for global localization. Instead of relying on appearances to describe local features, our method leverages high-level semantic scene understanding and large-scale context, which enables localization in noisy scenes. This is important since the number of detectable semantic classes is typically limited, leading to self-similarity when only considering single objects in isolation. We built up pipelines to extract *Descriptellation* from real-world point cloud data, and compared its global localization performance with handcrafted and learned constellation descriptors. The models are trained on simulation data for easy learning and data efficiency, but show good performance with a matching accuracy measured by the Top5 ratio close to 100% on simulation data, and a competitive localization success rate on real-world datasets.

## REFERENCES

- [1] R. Mur-Artal and J. Tardos, "ORB-SLAM2: An open-source SLAM system for monocular, stereo and RGB-D cameras," *IEEE Transactions on Robotics*, vol. PP, 10 2016.
- [2] D. Gálvez-López and J. D. Tardos, "Bags of binary words for fast place recognition in image sequences," *IEEE Transactions on Robotics*, vol. 28, no. 5, pp. 1188–1197, 2012.
- [3] D. G. Lowe, "Distinctive image features from scale-invariant keypoints," *International journal of computer vision*, vol. 60, no. 2, pp. 91–110, 2004.
- [4] H. Bay, T. Tuytelaars, and L. V. Gool, "Surf: Speeded up robust features," in *European conference on computer vision*. Springer, 2006, pp. 404–417.
- [5] M. Calonder, V. Lepetit, C. Strecha, and P. Fua, "Brief: Binary robust independent elementary features," in *European conference on computer vision*, 2010, pp. 778–792.
- [6] E. Rublee, V. Rabaud, K. Konolige, and G. Bradski, "ORB: An efficient alternative to SIFT or SURF," in *2011 International Conference on Computer Vision*, 2011, pp. 2564–2571.
- [7] S. Lowry, N. Sünderhauf, P. Newman, J. J. Leonard, D. Cox, P. Corke, and M. J. Milford, "Visual place recognition: A survey," *IEEE Transactions on Robotics*, vol. 32, no. 1, pp. 1–19, 2015.
- [8] W. Maddern, M. Milford, and G. Wyeth, "Capping computation time and storage requirements for appearance-based localization with cat-slam," in *2012 IEEE International Conference on Robotics and Automation*. IEEE, 2012, pp. 822–827.
- [9] F. Taubner, F. Tschopp, T. Novkovic, R. Siegwart, and F. Furrer, "Lcd-line clustering and description for place recognition," in *2020 International Conference on 3D Vision (3DV)*, 2020, pp. 908–917.
- [10] S. Yang and S. Scherer, "Cubeslam: Monocular 3-d object slam," *IEEE Transactions on Robotics*, vol. 35, no. 4, pp. 925–938, 2019.
- [11] L. Nicholson, M. Milford, and N. Sünderhauf, "Quadricslam: Dual quadrics from object detections as landmarks in object-oriented slam," *IEEE Robotics and Automation Letters*, vol. 4, no. 1, pp. 1–8, 2018.
- [12] F. Tschopp, J. Nieto, R. Siegwart, and C. Cadena, "Superquadric object representation for optimization-based semantic SLAM," *arXiv preprint arXiv:2109.09627*, 2021.
- [13] S. L. Bowman, N. Atanasov, K. Daniilidis, and G. J. Pappas, "Probabilistic data association for semantic slam," in *2017 IEEE international conference on robotics and automation (ICRA)*. IEEE, 2017, pp. 1722–1729.
- [14] F. Zhong, S. Wang, Z. Zhang, C. Chen, and Y. Wang, "Detect-slam: Making object detection and slam mutually beneficial," in *2018 IEEE Winter Conference on Applications of Computer Vision (WACV)*, 2018, pp. 1001–1010.
- [15] N. Sünderhauf, S. Shirazi, F. Dayoub, B. Upcroft, and M. Milford, "On the performance of ConvNet features for place recognition," in *2015 IEEE/RSJ International Conference on Intelligent Robots and Systems (IROS)*, 2015, pp. 4297–4304.
- [16] Y. Liu, Y. Petillot, D. Lane, and S. Wang, "Global localization with object-level semantics and topology," in *2019 International Conference on Robotics and Automation (ICRA)*. IEEE, 2019, pp. 4909–4915.
- [17] A. Gawel, C. Del Don, R. Siegwart, J. Nieto, and C. Cadena, "X-view: Graph-based semantic multi-view localization," *IEEE Robotics and Automation Letters*, vol. 3, no. 3, pp. 1687–1694, 2018.
- [18] T. N. Kipf and M. Welling, "Semi-supervised classification with graph convolutional networks," in *5th International Conference on Learning Representations, ICLR 2017, Toulon, France, April 24–26, 2017, Conference Track Proceedings*, 2017.
- [19] Y. Wang, Y. Sun, Z. Liu, S. E. Sarma, M. M. Bronstein, and J. M. Solomon, "Dynamic graph cnn for learning on point clouds," *Acm Transactions On Graphics (tog)*, vol. 38, no. 5, pp. 1–12, 2019.
- [20] S. Salti, F. Tombari, and L. D. Stefano, "SHOT: Unique signatures of histograms for surface and texture description," *Comput. Vis. Image Underst.*, vol. 125, pp. 251–264, 2014.
- [21] J. Guo, P. V. Borges, C. Park, and A. Gawel, "Local descriptor for robust place recognition using lidar intensity," *IEEE Robotics and Automation Letters*, vol. 4, no. 2, pp. 1470–1477, 2019.
- [22] R. Dubé, D. Dugas, E. Stumm, J. Nieto, R. Siegwart, and C. Cadena, "Segmatch: Segment based place recognition in 3d point clouds," in *2017 IEEE International Conference on Robotics and Automation (ICRA)*. IEEE, 2017, pp. 5266–5272.
- [23] R. Dubé, A. Cramariuc, D. Dugas, J. Nieto, R. Siegwart, and C. Cadena, "SegMap: 3d segment mapping using data-driven descriptors," *arXiv preprint arXiv:1804.09557*, 2018.
- [24] A. Cramariuc, F. Tschopp, N. Alatur, S. Benz, T. Falck, M. Brühlmeier, B. Hahn, J. Nieto, and R. Siegwart, "SemSegMap – 3d segment-based semantic localization," in *2021 IEEE/RSJ International Conference on Intelligent Robots and Systems (IROS)*, 2021, pp. 1183–1190.
- [25] R. Arandjelovic and A. Zisserman, "All about vlad," in *Proceedings of the IEEE conference on Computer Vision and Pattern Recognition*, 2013, pp. 1578–1585.
- [26] M. A. Uy and G. H. Lee, "Pointnetvlad: Deep point cloud based retrieval for large-scale place recognition," in *Proceedings of the IEEE Conference on Computer Vision and Pattern Recognition*, 2018, pp. 4470–4479.
- [27] M. Bosse and R. Zlot, "Place recognition using keypoint voting in large 3D lidar datasets," in *2013 IEEE International Conference on Robotics and Automation*, 2013, pp. 2677–2684.
- [28] X. Kong, X. Yang, G. Zhai, X. Zhao, X. Zeng, M. Wang, Y. Liu, W. Li, and F. Wen, "Semantic graph based place recognition for 3d point clouds," in *2020 IEEE/RSJ International Conference on Intelligent Robots and Systems (IROS)*. IEEE, 2020, pp. 8216–8223.
- [29] Z. Zhang, P. Cui, and W. Zhu, "Deep learning on graphs: A survey," *IEEE Transactions on Knowledge and Data Engineering*, vol. PP, pp. 1–1, 03 2020.
- [30] B. Perozzi, R. Al-Rfou, and S. Skiena, "DeepWalk: Online learning of social representations," *Proceedings of the ACM SIGKDD International Conference on Knowledge Discovery and Data Mining*, 03 2014.
- [31] A. Grover and J. Leskovec, "node2vec: Scalable feature learning for networks," in *Proceedings of the 22nd ACM SIGKDD international conference on Knowledge discovery and data mining*, 2016, pp. 855–864.
- [32] G. Nikolentzos, P. Meladianos, and M. Vazirgiannis, "Matching node embeddings for graph similarity," in *Proceedings of the Thirty-First AAAI Conference on Artificial Intelligence*, ser. AAAI'17, 2017, p. 2429–2435.
- [33] G. Li, M. Müller, A. Thabet, and B. Ghanem, "DeepGCNs: Can GCNs Go as Deep as CNNs?" in *The IEEE International Conference on Computer Vision (ICCV)*, 2019.
- [34] Y. Li, D. Tarlow, M. Brockschmidt, and R. Zemel, "Gated graph sequence neural networks," *arXiv preprint arXiv:1511.05493*, 2015.
- [35] A. Hermans\*, L. Beyer\*, and B. Leibe, "In Defense of the Triplet Loss for Person Re-Identification," *arXiv preprint arXiv:1703.07737*, 2017.
- [36] M. A. Fischler and R. C. Bolles, "Random sample consensus: a paradigm for model fitting with applications to image analysis and automated cartography," *Communications of the ACM*, vol. 24, no. 6, pp. 381–395, 1981.
- [37] D. Kingma and J. Ba, "Adam: A method for stochastic optimization," *International Conference on Learning Representations*, 12 2014.
- [38] X. Roynard, J.-E. Deschaud, and F. Goulette, "Paris-Lille-3D: A large and high-quality ground-truth urban point cloud dataset for automatic segmentation and classification," *The International Journal of Robotics Research*, vol. 37, no. 6, pp. 545–557, 2018.
- [39] B. Vallet, M. Brédif, A. Serna, B. Marcotegui, and N. Paparoditis, "TerraMobilita/iQmulus urban point cloud analysis benchmark," *Computers and Graphics*, vol. 49, pp. 126–133, 2015.
- [40] S. Katz, A. Tal, and R. Basri, "Direct visibility of point sets," *ACM Trans. Graph.*, vol. 26, no. 3, p. 24–es, Jul. 2007.
- [41] S. Vora, A. H. Lang, B. Helou, and O. Beijbom, "Pointpainting: Sequential fusion for 3d object detection," in *Proceedings of the IEEE/CVF conference on computer vision and pattern recognition*, 2020, pp. 4604–4612.
- [42] F. Tombari, S. Salti, and L. D. Stefano, "Unique signatures of histograms for local surface description," in *European conference on computer vision*. Springer, 2010, pp. 356–369.
- [43] Y. Zhu, Y. Ma, L. Chen, C. Liu, M. Ye, and L. Li, "Gosmatch: Graph-of-semantics matching for detecting loop closures in 3d lidar data," in *2020 IEEE/RSJ International Conference on Intelligent Robots and Systems (IROS)*, 2020, pp. 5151–5157.
- [44] C. R. Qi, H. Su, K. Mo, and L. J. Guibas, "Pointnet: Deep learning on point sets for 3d classification and segmentation," in *Proceedings of the IEEE conference on computer vision and pattern recognition*, 2017, pp. 652–660.